J. Fluid Mech. (1991), *vol.* 225, *pp.* 423–444
Printed in Great Britain

An investigation of transition to turbulence in bounded oscillatory Stokes flows Part 2. Numerical simulations

By R. AKHAVAN[1,2], R. D. KAMM[2] AND A. H. SHAPIRO[2]

[1] Department of Mechanical Engineering, The University of Michigan, Ann Arbor, MI 48109-2125

[2] Department of Mechanical Engineering, Massachusetts Institute of Technology, Cambridge, MA 02139

(Received 11 September 1989 and in revised form 26 September 1990)

The stability of oscillatory channel flow to different classes of infinitesimal and finite-amplitude two- and three-dimensional disturbances has been investigated by direct numerical simulations of the Navier–Stokes equations using spectral techniques. All infinitesimal disturbances were found to decay monotonically to a periodic steady state, in agreement with earlier Floquet theory calculations. However, before reaching this periodic steady state an infinitesimal disturbance introduced in the boundary layer was seen to experience transient growth in accordance with the predictions of quasi-steady theories for the least stable eigenmodes of the Orr–Sommerfeld equation for instantaneous 'frozen' profiles. The reason why this growth is not sustained in the periodic steady state is explained. Two-dimensional infinitesimal disturbances reaching finite amplitudes were found to saturate in an ordered state of two-dimensional quasi-equilibrium waves that decayed on viscous timescales. No finite-amplitude equilibrium waves were found in our cursory study. The secondary instability of these two-dimensional finite-amplitude quasi-equilibrium states to infinitesimal three-dimensional perturbations predicts transitional Reynolds numbers and turbulent flow structures in agreement with experiments.

1. Introduction

In Part 1 (Akhavan *et al.* 1991) experimental results on the structure of turbulent oscillatory flows in pipes were presented. From this work and similar studies on purely oscillatory flows conducted by other investigators in a variety of other geometries (Sergeev 1966; Merkli & Thomann 1975; Hino, Sawamoto & Takasu 1976; Ohmi *et al.* 1982; Hino *et al.* 1983), many features of the transition process in these flows have been identified. In particular, transition to turbulence has unanimously been observed at a Reynolds number based on Stokes boundary-layer thickness (Re^{δ}) of about 500 to 550, independent of the particular flow geometry (pipe, channel, oscillating plate). The resulting turbulent flow is characterized by the sudden, explosive appearance of turbulence towards the end of the acceleration phase of the cycle. Turbulent flow is sustained throughout the deceleration phase, while during the early stages of the acceleration phase production of turbulence essentially stops and velocity profiles agree with laminar theory. Nevertheless, during this period the disturbances retain a small but finite energy level.

These experimental observations are not in obvious accord with theory. It is

generally agreed that transition is due to the local instability of the Stokes boundary layers near the walls and, therefore, much of the existing theoretical work has addressed the stability of the basic Stokes layer. Theoretical work so far has been restricted to the study of infinitesimal disturbances, for which the equations of motion can be linearized; but even in this case the literature is not free of controversy. The difficulty lies with the time-dependent base velocity profile, which renders the time dependence of the disturbances inseparable and the method of normal modes formally inapplicable. One could, of course, neglect the time dependence of the base flow in the stability analysis and examine the stability of a succession of 'frozen' profiles (with a parametric dependence on time) by a normal mode approach. This would lead to a search for least-stable disturbances of the form $\boldsymbol{v}'(\boldsymbol{x},t) = \boldsymbol{v}'(z)\,\mathrm{e}^{\mathrm{i}(\alpha x+\beta y-\alpha c t)} + \text{c.c.}$ for the profile at a given phase during the cycle, where c is complex and the growth rates of the disturbances are given by $\mathrm{Im}\,(\alpha c)$. This quasi-steady approach has been favoured by a number of investigators (Collins 1963; Obremski & Morkovin 1969; Monkewitz & Bunster 1987; Cowley 1987), and is justified if one assumes that the instability of the Stokes layer arises from inflexion points of instantaneous velocity profiles. Since inflexional instabilities grow (or decay) on convective timescales ($t_{\mathrm{conv}} \sim \delta/U_0$), while in a Stokes layer the time variation of the base flow is by definition viscous ($T \sim 1/\Omega = \delta^2/\nu$), one would then be justified in neglecting the time variation of the base flow in the stability analysis. Obviously, since a variety of velocity profiles exist throughout a cycle, such a quasi-steady stability analysis would find the flow during certain portions of the cycle to be less stable than during others. For an oscillatory Stokes flow, such a quasi-steady stability analysis predicts the most dangerous profiles to occur near the start of the acceleration phase of the cycle with a critical $Re^{\delta} \sim 86$ (see for example, von Kerczek & Davis 1974). The least stable eigenmodes predicted by such a quasi-steady analysis have their peak energies around the inflexion points or the critical layers of the boundary layers near the walls. These predictions do not agree with experimental observations, which show that the flow becomes explosively unstable at the start of the deceleration phase of the cycle for $Re^{\delta} \sim 500$.

The second class of linear stability calculations proposed in the literature (von Kerczek & Davis 1974; Hall 1978) take advantage of the time-periodic nature of the base flow and extend the results of Floquet theory to obtain a description of the behaviour of the disturbances in the periodic steady state. A search is made for unstable disturbances of the form $\boldsymbol{v}'(\boldsymbol{x},\tau) = \tilde{\boldsymbol{v}}'(z,\tau)\,\mathrm{e}^{\mathrm{i}(\alpha x+\beta y)+\lambda\tau} + \text{c.c.}$, where $\tilde{\boldsymbol{v}}'(z,\tau)$ is a periodic function of time with the same periodicity as the base flow and λ is complex. The principal Floquet exponent, $\mathrm{Re}\,(\lambda)$, is a measure of the growth or decay of the disturbance from one cycle to the next. In all previous studies (von Kerczek & Davis 1974; Hall 1978) λ has been found to be real and negative, indicating that in the periodic steady state the oscillatory Stokes layer is absolutely stable to all infinitesimal disturbances. In addition, no evidence has been found of the growth of a disturbance within a cycle such that an infinitesimal disturbance could grow to finite amplitudes. Unlike quasi-steady theories, the least stable eigenmodes found by Floquet-theory calculations have their peak energies away from the walls. How these results relate to quasi-steady calculations has so far not been explained.

In the present work we would like to bridge some of the gap between theory and experiment by trying to identify a possible set of disturbances that could result in transitional Reynolds numbers, timescales of instability and turbulent flow structures similar to what has been observed in experiments. Our studies are based on direct numerical simulations of the Navier–Stokes equations using spectral

techniques, in which the evolution of the flow in the presence of a prescribed set of infinitesimal or finite-amplitude initial disturbances is followed.

2. Problem formulation and numerical methods

The flow geometry chosen for the numerical simulations is a two-dimensional channel, confined between rigid walls at $z^* = \pm h$ and infinite in extent in the streamwise, x^*, and spanwise, y^*, directions. For all the simulations, the Stokes parameter representing the ratio of channel half-width to Stokes-layer thickness was taken to be 10 ($\Lambda \equiv h/\delta \equiv h(\Omega/2\nu)^{\frac{1}{2}} = 10$). The flow rate per unit width into this channel was prescribed as $Q^* = -Q_0 \sin \Omega t$. The choice of a channel geometry for the numerical simulations as opposed to a pipe geometry for our experiments in Part 1 was mainly a matter of convenience, and was based on the close similarity between experimental results for different flow geometries.

The numerical schemes used in this study are similar to those used by Orszag & Kells (1980) and Orszag & Patera (1983) in earlier studies of transition to turbulence in steady wall-bounded shear flows. In this approach the stability of the flow is studied by solving numerically an initial-value problem that generally consists of the base flow plus a prescribed set of initial disturbances. Various details of the numerical schemes can be found in the literature (Orszag & Kells 1980; Orszag & Patera 1983). Here we summarize the basic discretization and time-stepping procedures.

The Navier–Stokes equations are solved in rotational form,

$$\frac{\partial \boldsymbol{v}^*}{\partial t} = \boldsymbol{v}^* \times \boldsymbol{\omega}^* - \boldsymbol{\nabla}\left(\frac{p^*}{\rho} + \tfrac{1}{2}|\boldsymbol{v}^*|^2\right) + \nu \nabla^2 \boldsymbol{v}^* + f^* \hat{\boldsymbol{x}}, \tag{1}$$

where $\boldsymbol{\omega}^* = \boldsymbol{\nabla} \times \boldsymbol{v}^*$ is the vorticity, $(p^*/\rho + |\boldsymbol{v}^*|^2/2)$ is the pressure head and $\hat{\boldsymbol{x}}$ denotes the unit vector in the x^*-direction. The mean pressure gradient is not included in p^* but is represented by the external forcing f^*. Here, * denotes dimensional quantities.

Introducing the non-dimensional quantities

$$\tau = \Omega t, \quad \boldsymbol{v} = \frac{\boldsymbol{v}^*}{U_0}, \quad \text{where} \quad U_0 = \frac{Q_0}{2h},$$

$$\boldsymbol{x} = \frac{\boldsymbol{x}^*}{\delta}, \quad \text{where} \quad \delta = \left(\frac{2\nu}{\Omega}\right)^{\frac{1}{2}}, \quad \Pi = \left(\frac{p^*}{\rho} + \tfrac{1}{2}|\boldsymbol{v}^*|^2\right)/U_0^2, \quad f = f^*/\left(\frac{U_0^2}{\delta}\right),$$

the non-dimensional form of the Navier–Stokes equations is obtained as

$$\frac{\partial \boldsymbol{v}}{\partial \tau} = \tfrac{1}{2} Re^{\delta}(\boldsymbol{v} \times \boldsymbol{\omega}) - \tfrac{1}{2}(Re^{\delta})\,\boldsymbol{\nabla}\Pi + \tfrac{1}{2}\nabla^2 \boldsymbol{v} + \tfrac{1}{2}(Re^{\delta}) f \hat{\boldsymbol{x}}. \tag{2}$$

This equation is solved together with the continuity equation

$$\boldsymbol{\nabla} \cdot \boldsymbol{v} = 0 \tag{3}$$

subject to no-slip boundary conditions at $z = \pm \Lambda$, and periodic boundary conditions in the streamwise and spanwise directions,

$$\boldsymbol{v}\left(x + \frac{2\pi n}{\alpha}, y + \frac{2\pi m}{\beta}, z, \tau\right) = \boldsymbol{v}(x, y, z, \tau),$$

where α and β are specified streamwise and spanwise wavenumbers.

	Frozen profile at $\Omega t = 0$		Frozen profile at $\Omega t = \pi/2$	
	2D disturbance	3D disturbance	2D disturbance	3D disturbance
Re^δ	1000	$1000\sqrt{2}$	1000	$1000\sqrt{2}$
α	0.5	$0.5/\sqrt{2}$	0.5	$0.5/\sqrt{2}$
β	—	$0.5/\sqrt{2}$	—	$0.5/\sqrt{2}$
Re (αc)	−0.06858357	−0.04849591	0.54467293	0.38514192
Im (αc)	0.02015786	0.01425378	0.00175319	0.00121291
Resolution $2N \times (P+1)$	8×65	8×65	8×65	8×65
Courant no.	0.1	0.1	0.1	0.1
Final time	$\pi/10$	$\pi/10$	$\pi/2+\pi/10$	$\pi/2+\pi/10$
Predicted amp. change $e^{(Re/2)\,\mathrm{Im}\,(\alpha c)\,t}$	23.722	23.722	1.309	1.309
Computed amp. change	23.406	23.446	1.346	1.341
Predicted phase change $e^{-i(Re/2)\,\mathrm{Re}\,(\alpha c)\,t}$	10.773°	10.773°	−85.557°	−85.557°
Computed phase change	10.772°	10.772°	−85.813°	−85.813°

TABLE 1. Comparison of the evolution of small-amplitude disturbances for frozen profiles to predictions from the Orr–Sommerfeld equation

In the spectral discretization the velocity is represented using Chebyshev polynomials in z and Fourier series in x and y,

$$v = \sum_{p=0}^{P} \sum_{n=-N}^{N} \sum_{m=-M}^{M} v_{nmp}(\tau)\, e^{i\alpha n x} e^{i\beta m y} T_p(z).$$

The time-stepping scheme used in the solution of (2) is a fractional-step (splitting) method (Orszag & Patera 1983) consisting of an explicit (second-order Adams–Bashforth) convective step, a pressure step where incompressibility is imposed, and an implicit (Euler-backward) step to incorporate viscous effects and impose viscous boundary conditions. Implementation of the imposed flow rate, $Q = -\sin \Omega t$, is achieved by a Green's function method as described in Akhavan (1987).

Initial conditions for the runs reported in this study generally consisted of the base laminar flow on which various combinations of infinitesimal or finite-amplitude two- or three-dimensional perturbations (corresponding to the least stable eigenmodes of the Orr–Sommerfeld equation for the 'frozen' initial profile) were superimposed. The evolution of the disturbances were tracked by following the energies of the two- and three-dimensional perturbations,

$$E_2 = \sum_{n=1}^{N} \frac{1}{2\Lambda} \int_{-\Lambda}^{\Lambda} (v_n^{(2)} \cdot v_n^{*(2)})\, dz, \tag{4}$$

$$E_3 = \sum_{m=-M}^{M} \sum_{n=0}^{N} \frac{1}{2\Lambda} \int_{-\Lambda}^{\Lambda} (v_{nm}^{(3)} \cdot v_{nm}^{*(3)})\, dz. \tag{5}$$

A number of tests were performed to verify the accuracy of our numerical schemes. An example of these tests is shown in table 1, where the computed growth rates from direct simulations for the least-stable eigenmodes of two different 'frozen' profiles are compared to values predicted by an eigenvalue solution of the Orr–Sommerfeld equation for the same 'frozen' profiles.

Typical parameter values for direct simulations were $P = 64$ (or 128), $2N = 32$, $2M = 2$, Courant number = 0.1. Convergence in all these parameters has been verified by either halving or doubling the resolution.

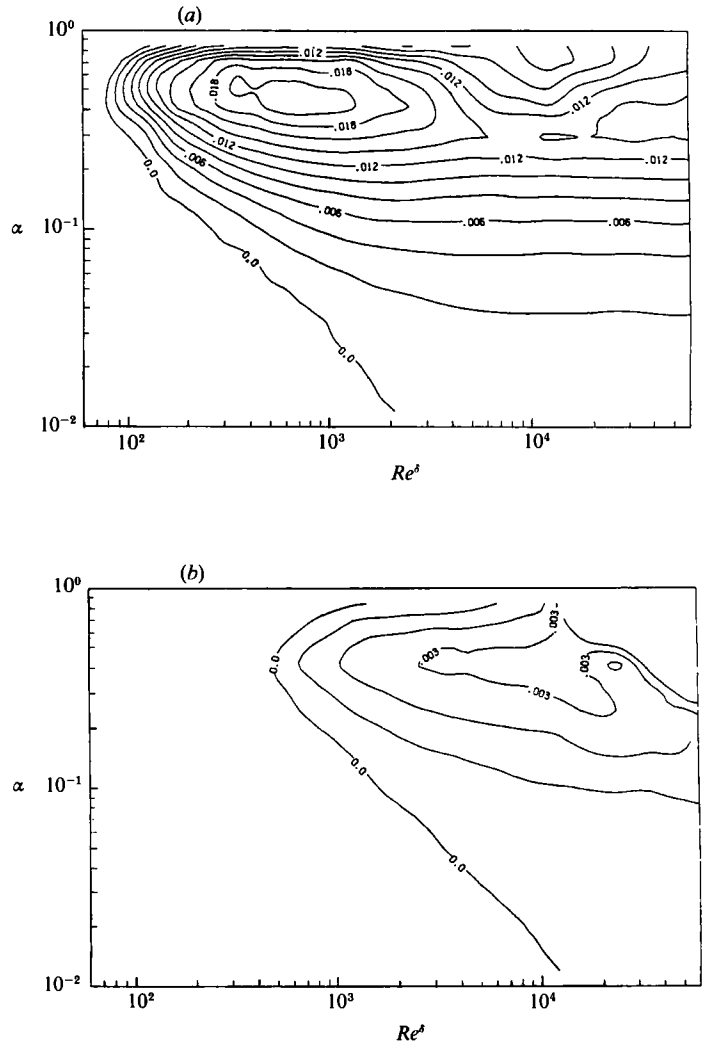

FIGURE 1. Iso-growth curves for the 'frozen' profiles at (*a*) $\Omega t = 0$ and (*b*) $\Omega t = \frac{1}{2}\pi$.

3. Infinitesimal disturbances

In this section we present results obtained for the evolution of small-amplitude (infinitesimal) disturbances. To save on computational time, the evolution of infinitesimal disturbances was tracked by solving the linearized Navier–Stokes equations instead of the full nonlinear problem. The linearized equations were obtained by assuming a velocity field of the form

$$\boldsymbol{v}(\boldsymbol{x},\tau) = \bar{U}(z,\tau)\,\hat{\boldsymbol{x}} + \epsilon \boldsymbol{v}'(\boldsymbol{x},\tau) \quad (\epsilon \ll 1) \tag{6}$$

and retaining only terms of order ϵ in the Navier–Stokes equations (2). The resulting linearized equations are

$$\frac{\partial}{\partial \tau}(u', v', w') = -\tfrac{1}{2}Re^\delta(\bar{U}u'_x + w'\bar{U}_z,\ \bar{U}v'_x, \bar{U}w'_x) - \tfrac{1}{2}Re^\delta(\Pi'_x, \Pi'_y, \Pi'_z) + \tfrac{1}{2}\nabla^2(u', v', w'), \tag{7}$$

where $\boldsymbol{v}'$ is the disturbance velocity and $\bar{U}(z,\tau)$ is the laminar base velocity. In the

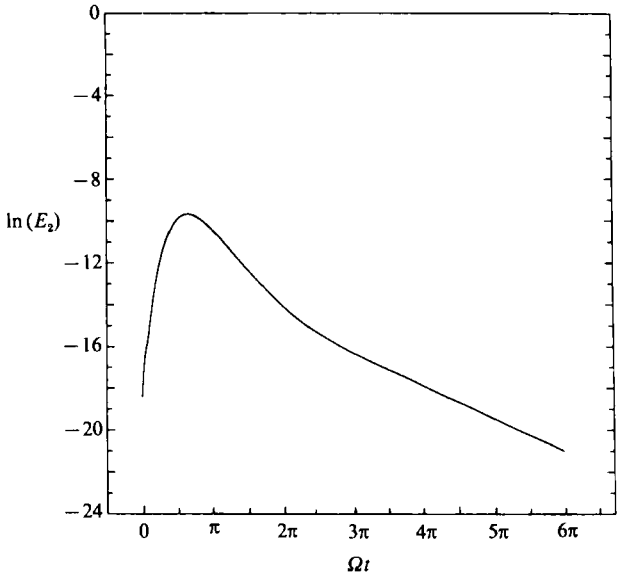

FIGURE 2. Evolution of the energy of a two-dimensional disturbance at $Re^{\delta} = 1000$, $\alpha = 0.5$. The simulation was started at $\Omega t = 0$ and the initial disturbance is the least-stable eigenmode for the profile at this instant.

formulation of $\boldsymbol{v}'$ only one Fourier mode is kept in the streamwise (and spanwise, in the case of three-dimensional disturbances) direction owing to linearity and separability. Except for the implementation of the nonlinear terms, the method of solution is identical to that described in §2. The accuracy of the solution has been verified by comparing the results of the linearized problem to that of the full simulation for a test case ($Re^{\delta} = 1000$, $\alpha = 0.5$, two-dimensional disturbance).

For planar geometries it can be shown (von Kerczek & Davis 1974) that Squires theorem holds in the usual manner, relating the evolution of any three-dimensional infinitesimal disturbance to a two-dimensional disturbance at a lower Reynolds number. The first instability is, therefore, expected to be two-dimensional. Consequently only two-dimensional disturbances will be considered.

Before discussing the results of time-dependent simulations for the evolution of infinitesimal disturbances, we will briefly consider the predictions of a quasi-steady calculation for the same problem. These results were obtained by a spectral solution of the Orr–Sommerfeld equation (Orszag 1971), and are shown in figure 1 for the profiles at two phases during the cycle; one the profile at the start of the acceleration phase ($\Omega t = 0$) and the other, the profile at start of the deceleration phase ($\Omega t = \frac{1}{2}\pi$). As seen in figure 1, a stability analysis of this kind predicts the profiles near the start of the acceleration phase to be more dangerous than those near the start of the deceleration phase, and estimates the critical Reynolds number (Re^{δ}) to be ~ 85. Both these features are in conflict with experimental observations which show that the flow becomes turbulent at the start of the deceleration phase with $Re^{\delta}_{\text{crit}} \sim 500$. For both phases $\Omega t = 0$ and $\frac{1}{2}\pi$, however, the stability maps of figure 1 show the most unstable streamwise wavenumbers to be located near $\alpha \sim 0.5$. If the quasi-steady problem is at all relevant to the problem of stability of oscillatory Stokes layers, the stability maps of figure 1 suggest a search for unstable modes in the range of wavenumbers $\alpha \sim 0.2$–0.7.

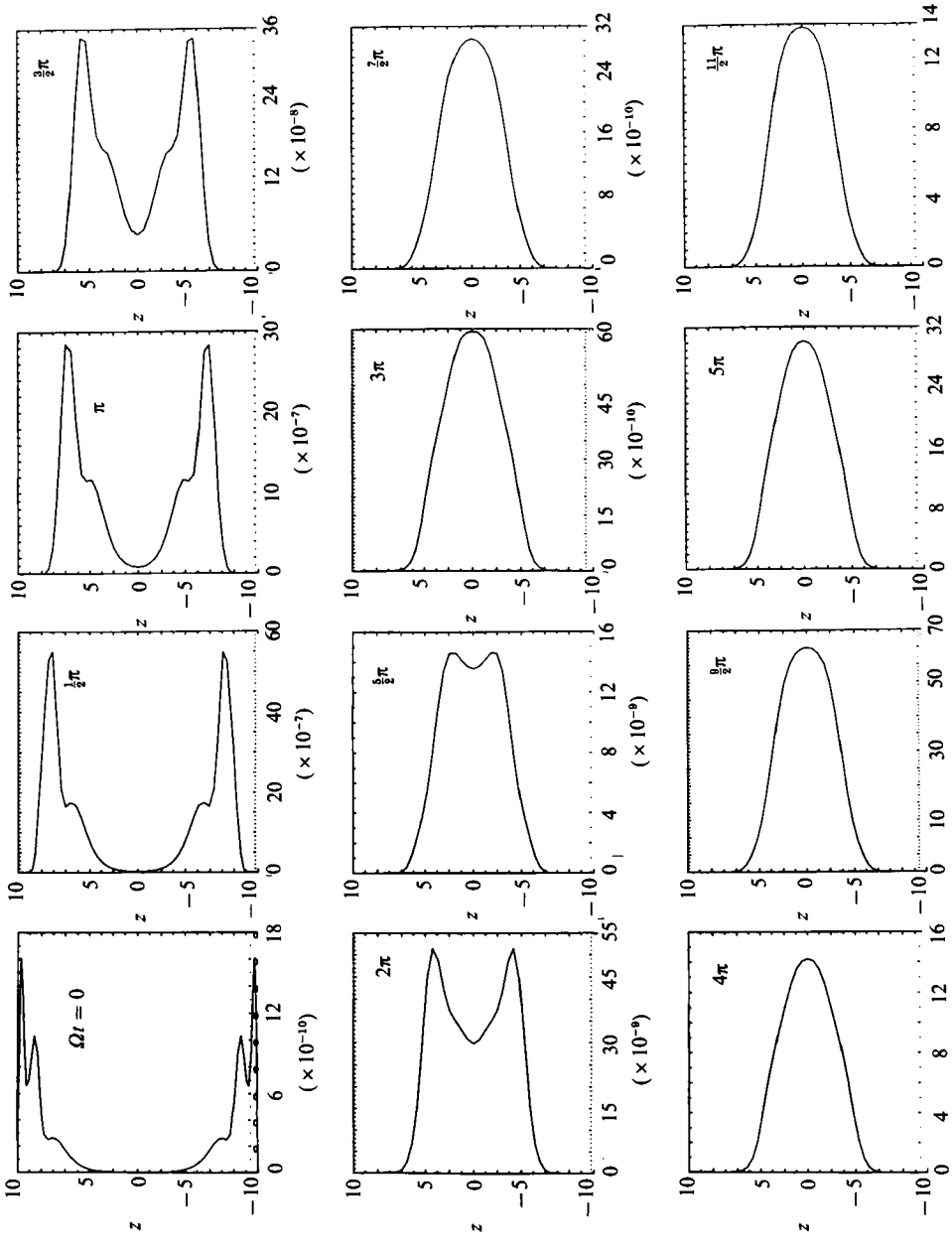

FIGURE 3. Distributions of the energy of disturbances across the channel width for selected times during the simulation. The simulation was started at $\Omega t = 0$ and the initial disturbance is the least-stable eigenmode for the profile at this instant. ($Re' = 1000$, $\alpha = 0.5$.)

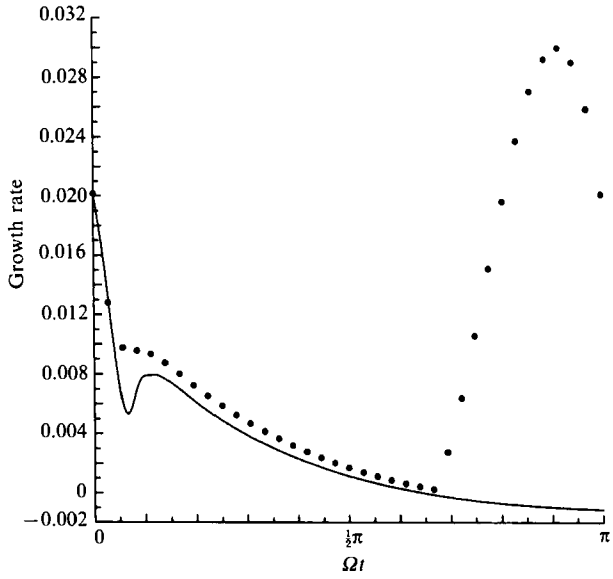

FIGURE 4. Comparison of the growth rates from the direct simulation (solid line) to the growth rates of the least-stable eigenmodes of the Orr–Sommerfeld equation for the 'frozen' profiles at each instant (symbols). (Two-dimensional disturbance, $Re^{\delta} = 1000$, $\alpha = 0.5$.)

Next we will consider the results of direct simulations for the evolution of infinitesimal disturbances. The initial disturbance for these simulations is specified as the least-stable eigenmode of the initial 'frozen' profile. The evolution of this disturbance, however, is tracked by the time-dependent Navier–Stokes equations. In the periodic steady state, therefore, our results should agree with the results obtained by Floquet theory.

The results of such a simulation for a channel flow at $Re^{\delta} = 1000$ subjected to a two-dimensional initial disturbance with $\alpha = 0.5$ are shown in figures 2 and 3. The flow is started at a time of $\Omega t = 0$ corresponding to zero flow rate. The initial disturbance is prescribed as the least-stable eigenmode of the Orr–Sommerfeld equation for the initial profile, and is normalized to have an energy, E_2, of 10^{-8} relative to that of the mean flow. In figure 2, the evolution of the overall energy of the disturbance is tracked as a function of time. It can be seen that the disturbance experiences an initial period of transient growth which is followed by a state of monotonic decay in the periodic steady state. The reason why the initial transient growth is not sustained in the periodic steady state can be seen in figure 3, where the distributions of the energy of the disturbances across the channel width are plotted for selected times during the simulation. The initial disturbance is seen to have its peak energy around the critical layers near the walls, with two less prominent peaks at successive inflexions points further away. For the first half-period or so ($0 < \Omega t < 8\pi/10$), the disturbances evolve in ways not too different from what would be predicted by quasi-steady theories; at each instant in time the disturbance simply locks on to the least-stable eigenmode of the Orr–Sommerfeld equation for the profile at that instant. During this period, both the growth rates and the distributions of the energy of the disturbances across the channel width are identical to what would be predicted by quasi-steady theories. In figure 4, the growth rates observed in the direct simulation are compared to the growth rates of the least-

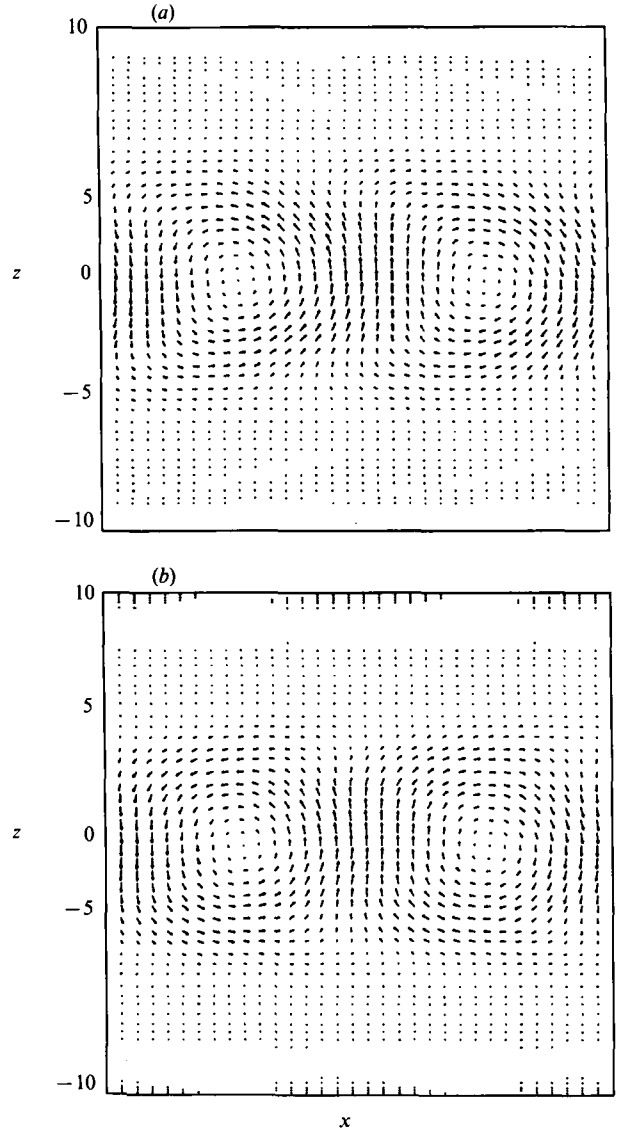

FIGURE 5. The disturbance field in the periodic steady state as seen in a frame of reference moving with the centreline velocity. ($Re^s = 1000$, $\alpha = 0.5$.) (*a*) $\Omega t = \frac{7}{2}\pi$, (*b*) $\Omega t = 4\pi$.

stable eigenmodes for 'frozen' profiles at each phase during the first half-cycle. The two growth rates are seen to be in agreement for $0 < \Omega t < 8\pi/10$, but to diverge thereafter. The reason for this divergence can be understood from the plots of figure 3, where it can be seen that in its evolution from $\Omega t = 0$ to $\frac{1}{2}\pi$ and in the process of locking on to the least-stable eigenmodes at various phases, the disturbance has moved further away from the walls. Consequently, after the first half-cycle (say at a time of $\Omega t = \pi$), the disturbance is too far away from the walls to be able to excite the same modes that were excited half a period ago. Instead, it excites modes that are local to the disturbance (recall that the infinite Stokes layer has an infinite number of inflexion points, the strength of which drops off exponentially as a function of the distance from the walls). This 'mode-hopping' continues until the

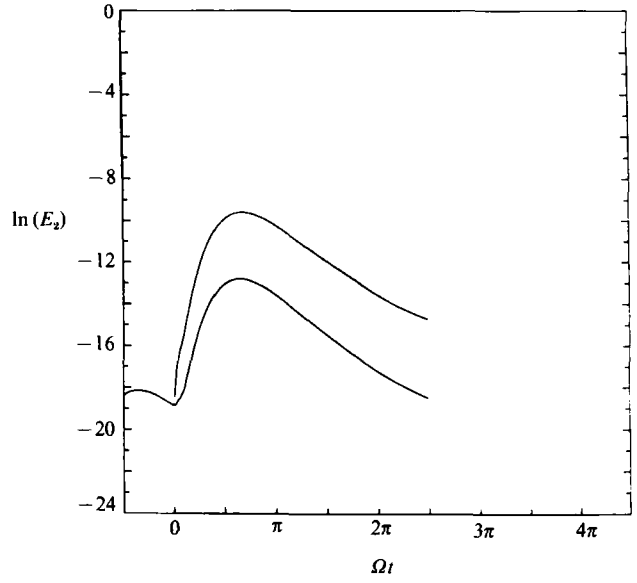

FIGURE 6. Evolution of the energy of a two-dimensional disturbance at $Re^{\delta} = 1000$, $\alpha = 0.5$ for two distinct initial conditions. At large times the growth rates become independent of the initial conditions.

disturbance has moved all the way to the centre of the channel, at which point it settles into a periodic steady state of monotonic decay. It is this steady-state behaviour that a Floquet analysis of the time-dependent Orr–Sommerfeld equation predicts.

In the periodic steady state, the disturbances are synchronous with the base flow; i.e. the disturbance at time $\Omega t + 2\pi$ differs from that at time Ωt only by an exponential factor (with no phase change). This means that the Floquet exponents are real, in agreement with the results found by von Kerczek & Davis (1974). This is to be expected since, as shown by von Kerczek & Davis (1974), if λ is an eigenvalue so should be its complex conjugate, λ^*. Thus the solution should either consist of pairs of simultaneous disturbance waves that propagate in opposite directions, or else it should be of the form of a standing wave $\tilde{v}' e^{i\alpha x + \lambda \tau}$, where λ is real. Furthermore, the results from the numerical simulations show that in the periodic steady state, the disturbance field is stationary in a frame of reference moving with the centreline velocity (figure 5).

While the initial transient behaviour of the disturbances is dependent upon the specific form of the initial disturbance and the phase in the cycle at which the simulation is started, the behaviour in the periodic state is independent of these initial conditions. This can be seen in figures 6 and 7 which show the results for the same problem with the simulation started at $\Omega t = -\frac{1}{2}\pi$ and the flow subjected to an initial disturbance that is the least-stable eigenmode of the Orr–Sommerfeld equation for the profile at $\Omega t = -\frac{1}{2}\pi$. As can be seen from a comparison of these figures and figures 2 and 3, for large times both the growth rates and the distributions of the energies of the disturbances across the channel width are identical for the two simulations. The initial transient behaviour of the disturbances shown in figure 7 is also of interest. In particular, note the competition between the two modes at $\Omega t = 0$ in figure 7. Since the inflexion points near the walls are much stronger than the ones

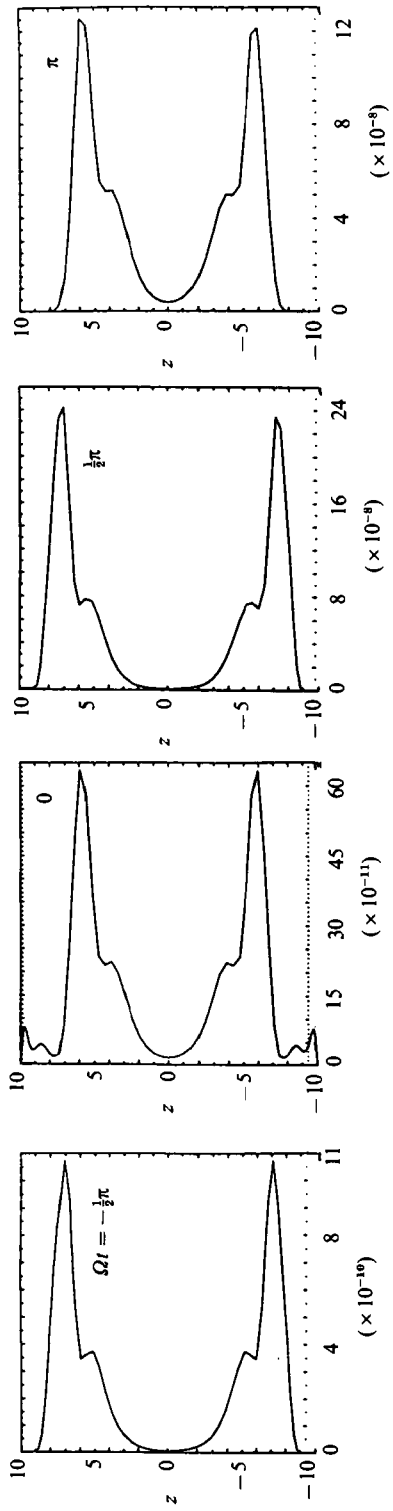

FIGURE 7. Distributions of the energy of disturbances across the channel width at $Re' = 1000$, $\alpha = 0.5$ for the simulation started at $\Omega t = -\frac{1}{2}\pi$. At large times these distributions are identical to the distributions shown in figure 3.

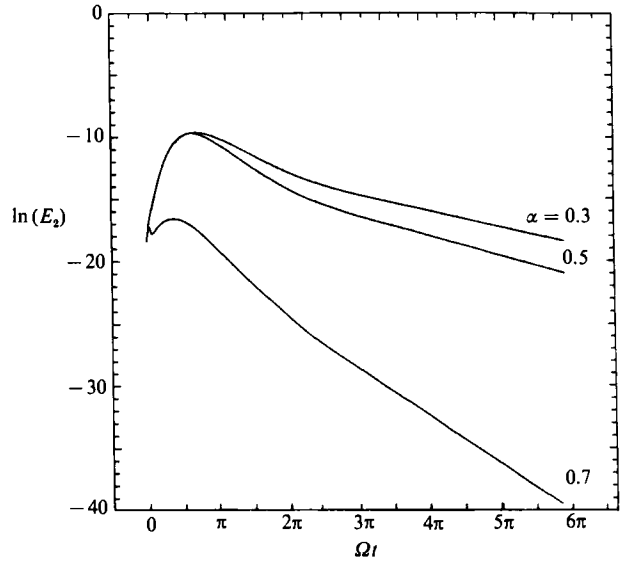

FIGURE 8. Evolution of two-dimensional disturbances with streamwise wavenumbers $\alpha = 0.3$, 0.5 and 0.7 at $Re^\delta = 1000$.

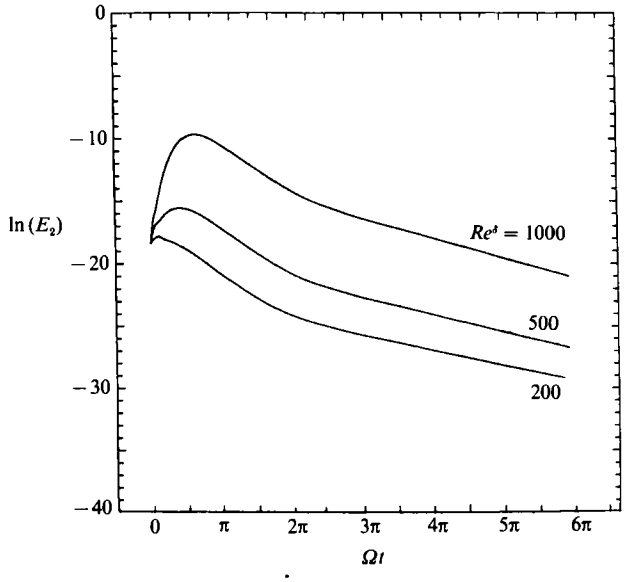

FIGURE 9. Evolution of two-dimensional disturbances with $\alpha = 0.5$ at $Re^\delta = 200$, 500 and 1000.

further away, whenever there is any residual disturbance in the near-wall region the near-wall modes are triggered. This is the case at $\Omega t = 0$ but not the case at $\Omega t = \pi$ of figure 7.

The results of the simulation for other values of Re^δ and streamwise wavenumber α are shown in figures 8 and 9. In each case the evolution of the disturbance is similar to the case discussed above; after an initial transient period of growth the disturbance migrates to the centre of the channel where it decays on viscous timescales. The resulting Floquet exponents are plotted in figure 10. The general

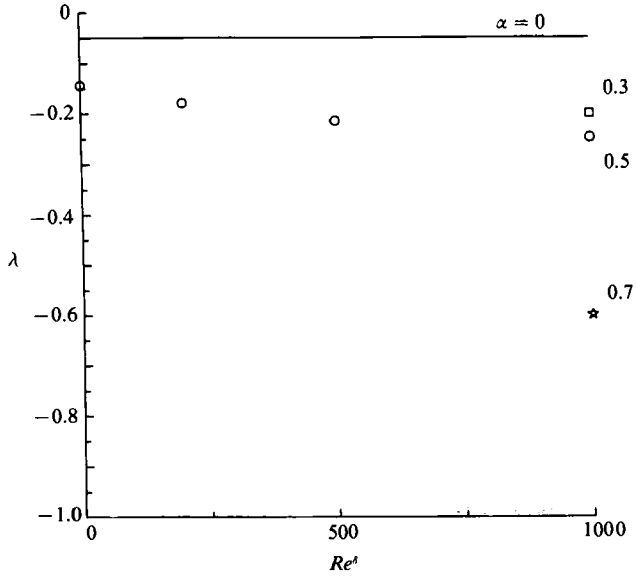

FIGURE 10. The variation of the principal Floquet exponent, λ, as a function of Re^δ and α.

trends in the behaviour of λ as a function of Re^δ and α are identical to those obtained by von Kerczek & Davis (1974, their figure 3) for a truncated flat Stokes layer, but the absolute magnitudes of λ are smaller.

For comparison to experimental measurements the transient behaviour of disturbances is more relevant than the Floquet-theory results, because in an experimental setting a certain level of noise is always present throughout the flow field. In this case, as we have seen, the disturbances can experience significant growth rates during the acceleration phase of the cycle. This may be the origin of the 'distorted laminar flows' that have been reported by Hino *et al.* (1976), where small-amplitude disturbances were observed superimposed on the laminar profiles during the acceleration phase of the cycle.

The transition process at $Re^\delta \sim 500$, however, cannot be explained by infinitesimal disturbances. The transient growth of infinitesimal disturbances at the start of the acceleration phase of the cycle provides a means by which a disturbance can grow to finite amplitudes, after which nonlinear phenomena need to be considered. This will be considered in the next section.

4. Finite-amplitude disturbances

4.1. *Two-dimensional primary instability*

We start with a consideration of two-dimensional disturbances of finite amplitude. Even though a two-dimensional theory cannot explain all the details of transition (in particular its three-dimensionality), an understanding of the two-dimensional behaviour is important because transition to turbulence in many examples of 'steady' wall-bounded and free-shear flows including free-shear layers (Pierrehumbert & Widnall 1982), plane Poiseulle flow (Herbert 1976, 1983; Orszag & Patera 1983), pipe and plane Couette flows (Orszag & Patera 1983) and boundary-layer flows (Herbert 1984) have been shown to be the result of secondary instability of two-dimensional finite-amplitude equilibrium (or quasi-equilibrium) waves to infinitesimal three-dimensional disturbances.

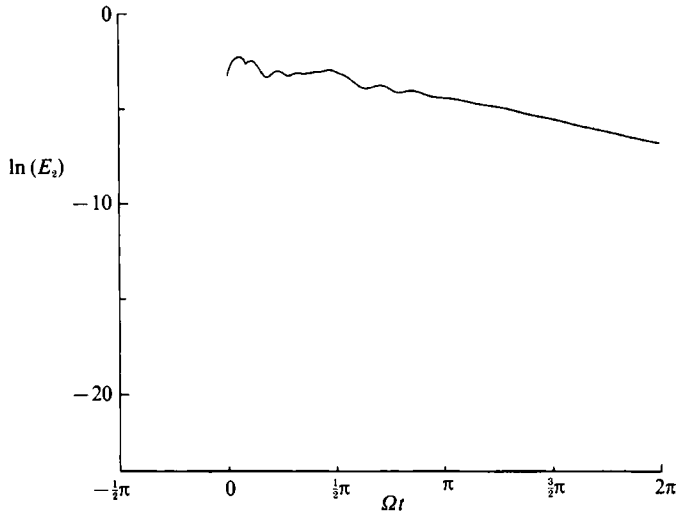

FIGURE 11. Evolution of the energy of a two-dimensional finite-amplitude disturbance at $Re^\delta = 1000$, $\alpha = 0.5$.

We will once again utilize direct numerical simulations of the Navier–Stokes equations to follow the evolution of the flow subjected to a finite-amplitude two-dimensional initial disturbance. Since the finite-amplitude disturbance is expected to arise from the nonlinear saturation of infinitesimal disturbances during their transient initial behaviour and since infinitesimal disturbances have their maximum transient growths around a wavenumber of $\alpha \approx 0.5$ we will consider the finite-amplitude behaviour of a disturbance with $\alpha = 0.5$ at a Reynolds number of 1000. The initial disturbance is specified to be in the form of the least-stable eigenmode of the Orr–Sommerfeld equation and is normalized to have an energy, E_2, of 0.04 relative to that of the mean flow. The simulations were obtained with a resolution $P = 128$, $2N = 32$.

The results of the simulation for the case $\alpha = 0.5$ are shown in figures 11–13. Of particular interest is whether the disturbances evolve to an equilibrium state, or decay, and in that case what the timescales of decay are. Figure 11 is a plot of the evolution of the energy of the disturbances as a function of time. After an initial transient period, the disturbances are seen to settle into a state of slow decay with viscous decay rates ($\lambda = -0.38$ on viscous timescales). The development of the disturbances can be seen in more detail in figure 12, where the distribution of the energy of the disturbance across the channel width is shown for selected times during the simulation. The initial disturbance field is localized near the walls with a major energy peak near the (linear) critical layer and two less prominent peaks at neighbouring inflexion points. Within a short time (on convective timescales) the disturbances migrate to the centre of the channel and settle into a quasi-equilibrium state where they are convected back and forth with the mean flow, maintaining their energy to $O(1/Re)$. Both the disturbance field and the attenuation rate, λ, are not too different from the Floquet-theory results of linear theory. Nonlinear effects tend to spread out the perturbation over a wider section of the cross-section and to result in slightly larger values of λ ($\lambda = -0.38$ for finite-amplitude disturbances at $\alpha = 0.5$ as compared to $\lambda = -0.25$ for the linear case).

The distortion of the mean velocity profiles due to the presence of these

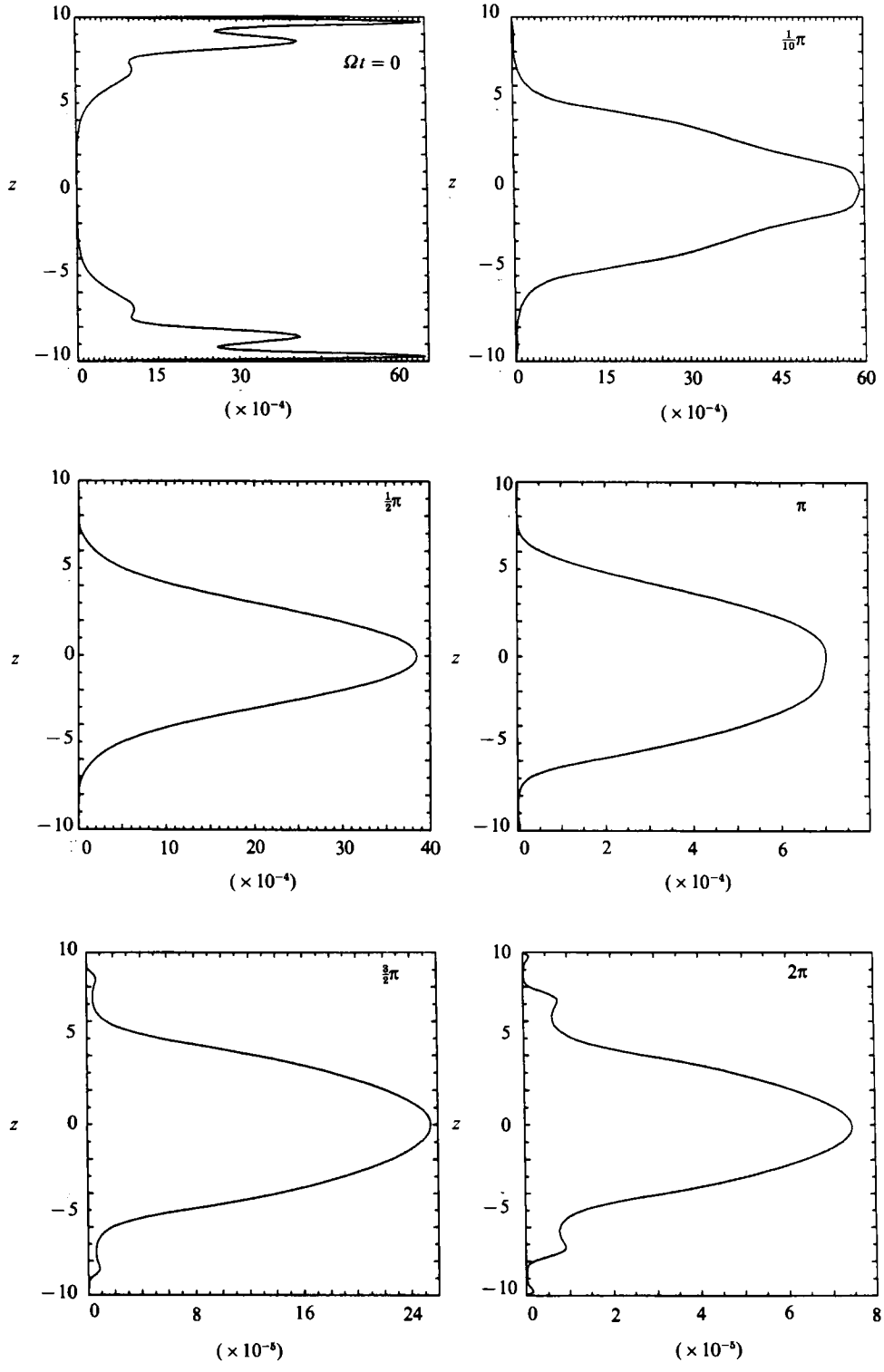

FIGURE 12. Distributions of the energy of two-dimensional finite-amplitude disturbances across the channel width for selected times during the simulation at $Re^{\delta} = 1000$, $\alpha = 0.5$.

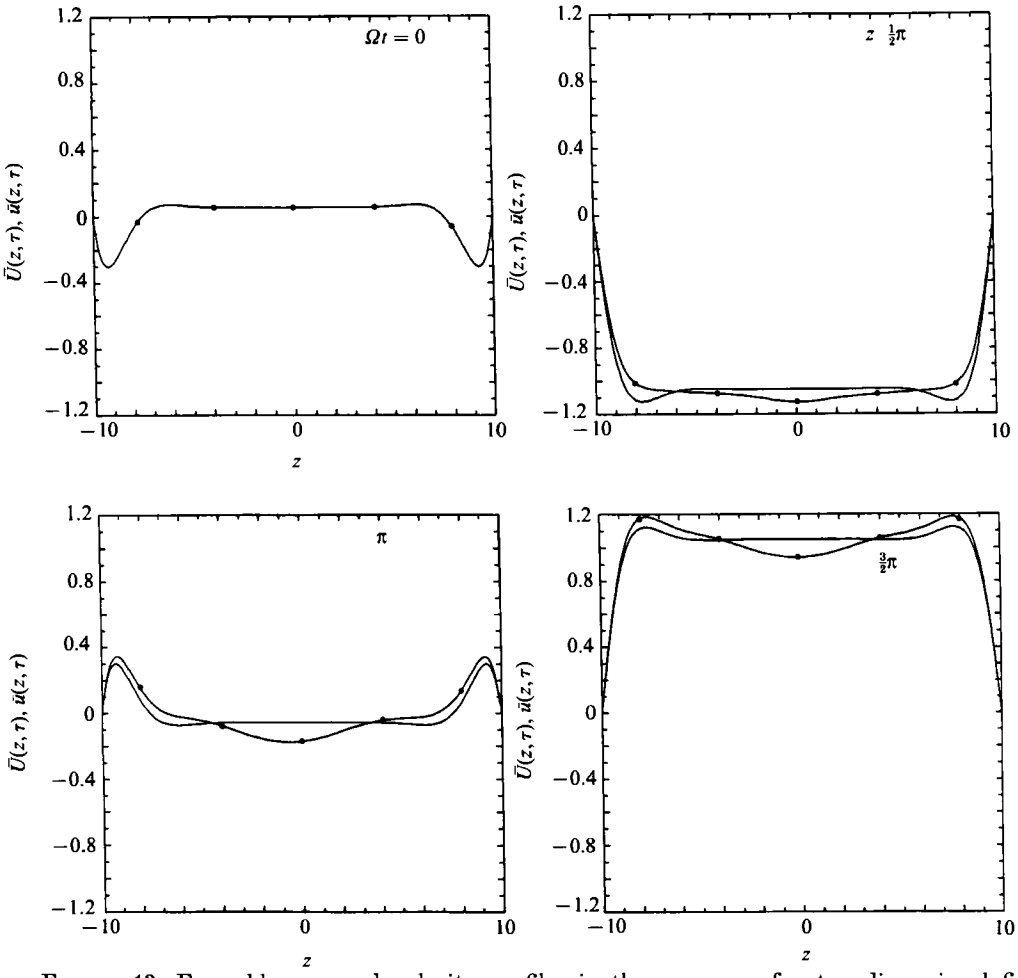

FIGURE 13. Ensemble-averaged velocity profiles in the presence of a two-dimensional finite-amplitude disturbance (—●—) compared to laminar profiles. ($Re^{\delta} = 1000$, $\alpha = 0.5$.)

disturbances is shown in figure 13. The largest effect occurs near the centre of the channel and away from the boundary layers, as this is where the disturbances are localized.

Similar simulations were performed for wavenumbers $\alpha = 0.3$ and 0.7, both at $Re^{\delta} = 1000$. In both cases the decay of the two-dimensional finite-amplitude wave was faster than the case $\alpha = 0.5$. Since the secondary instability mechanism described in the next section requires a two-dimensional finite-amplitude wave that retains its energy, the case $\alpha = 0.5$ has been chosen for the remaining calculations.

4.2. *Linear secondary instability*

When only two-dimensional disturbances are allowed the flow, as we have seen, evolves to a quasi-equilibrium state of travelling waves that decay over viscous timescales. If no further interactions with other disturbances take place, this flow remains well ordered at all times and shows no sign of the chaotic small-scale structure of real turbulent flows. However, in the presence of infinitesimal three-dimensional disturbances, the two-dimensional finite-amplitude flow is susceptible to an inviscid, large-growth-rate, broadband, spanwise excitation. This secondary

instability provides a plausible mechanism by which the abrupt nature of transition to turbulence in a wide variety of shear flows (including plane shear layers, plane Poiseulle flow, pipe and plane Couette flow and boundary-layer flow) can be explained.

A general understanding of this secondary instability mechanism has recently been achieved by inviscid (Pierrehumbert 1986; Bayly 1986) as well as viscous (Landman & Saffman 1987) arguments. It has been shown that in all these shear flows, the existence of the two-dimensional finite-amplitude wave leads to vortical structures within the flow which (in approximate form) can locally be described by elliptical streamlines. These elliptical eddy flows are inviscidly unstable (Pierrehumbert 1986; Bayly 1986; Landman & Saffman 1987) to three-dimensional perturbations over a large range of spanwise wavenumbers (with a spanwise wavenumber cutoff only due to the action of viscosity). The broadband nature of this instability (large spanwise wavenumber viscous cutoff) is very significant in the problem of transition to turbulence in shear flows, as it provides a means by which arbitrarily small scales can abruptly be generated from a smooth basic state.

The instability is dependent critically on the existence and persistence of the two-dimensional finite-amplitude wave at transitional Reynolds numbers, and is otherwise independent of the details of the flow such as the shape of the velocity profiles or the amplitude of the two-dimensional finite-amplitude wave (as long as the amplitude is above some critical value, i.e. it is finite). The energetic role of the two-dimensional finite-amplitude wave in the secondary instability process has been investigated by Orszag & Patera (1983). It has been shown that the two-dimensional finite-amplitude wave does not directly supply energy to the three-dimensional component. It merely acts as a 'catalyst', mediating the transfer of energy from the mean flow to the three-dimensional disturbance by continuously tilting the three-dimensional mean vorticity so that effective stretching can be achieved, leading to exponential growth of the three-dimensional disturbance.

We will, therefore, investigate the secondary instability of the primary two-dimensional state described in the previous section to infinitesimal three-dimensional perturbations. Once again, we will employ direct numerical simulations of the full time-dependent Navier–Stokes equations for our investigation. In particular, we will study the time evolution of flows resulting from initial conditions

$$\boldsymbol{v}(\boldsymbol{x}, t = 0) = \bar{U}\hat{x} + \boldsymbol{v}_{2\mathrm{D}} + \epsilon \boldsymbol{v}_{3\mathrm{D}},$$

where $\bar{U}$ is the basic laminar flow, $\boldsymbol{v}_{2\mathrm{D}}$ is the initial finite-amplitude two-dimensional disturbance with wave vector $(\alpha, 0)$ which is specified to be in the form of the least-stable eigenmode of the Orr–Sommerfeld equation for the initial profile and is normalized to have an energy, E_2, of 0.04 relative to that of the mean flow, and $\boldsymbol{v}_{3\mathrm{D}}$ is the initial three-dimensional disturbance which has the form of a streamwise vortex with wave vector $(0, \beta)$ and has a total energy of 10^{-8} relative to the mean flow. The calculations were performed with $P = 128$, $2N = 32$, $2M = 2$. Only one mode is kept in the spanwise direction owing to linearity and separability. The wavenumber of the two-dimensional finite-amplitude wave was chosen to be $\alpha = 0.5$.

The stability of this flow to disturbances with various spanwise wavenumbers β at a Re^{δ} of 1000 is shown in figure 14. To begin with, the simulations verify that there is indeed a strong three-dimensional instability. The three-dimensional disturbance grows in magnitude by a factor of 10 in the time it takes the fluid to travel 5 channel widths at maximum bulk velocity. This corresponds to a convective growth rate and suggests that the instability mechanism is inviscid.

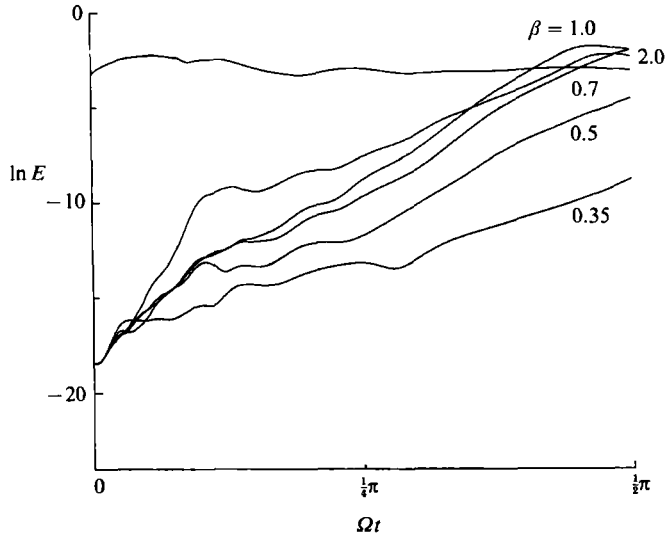

FIGURE 14. Spanwise wavenumber dependence of the three-dimensional growth rate. ($Re^{\delta} = 1000$, $\alpha = 0.5$.)

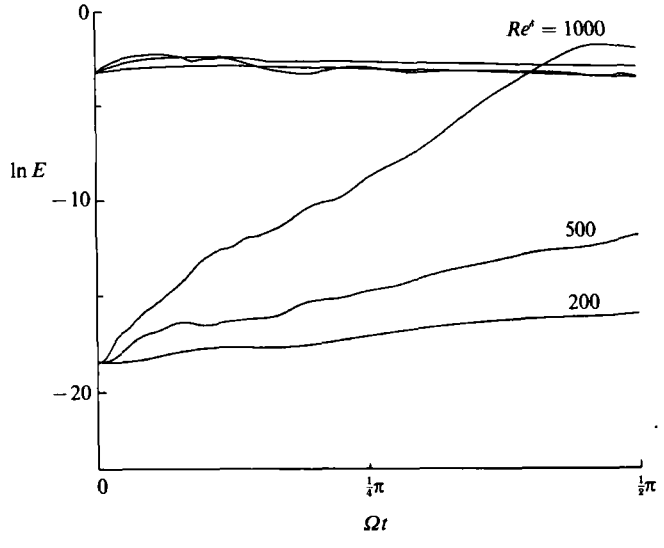

FIGURE 15. Reynolds-number dependence of the three-dimensional growth rate for flow with $\alpha = 0.5$, $\beta = 1.0$.

Secondly, the instability is effective for a large range of spanwise wavenumbers $\beta \sim O(1)$, emphasizing the broadband nature of the instability. There is a weak maximum in the magnitude of the growth rate at $\beta \approx 1$, but beyond that the preference in β is weak.

Finally, we need to show that the instability described above cuts off at $Re^{\delta} \approx 500$, which is the experimentally observed value for the transition Reynolds number. This is demonstrated in figure 15, where the evolution of the two-dimensional quasi-equilibrium state in the presence of an infinitesimal three-dimensional perturbation is followed at Reynolds numbers of 200, 500 and 1000 for $\alpha = 0.5$ and $\beta = 1.0$. Note

that a Reynolds number on the order of 500 is singled out as the critical Reynolds number below which three-dimensional disturbances cannot grow to finite amplitudes. Since the rate of decay of the two-dimensional wave is roughly the same at all three Reynolds numbers, we conclude that the cutoff is mainly due to viscous damping of the three-dimensional perturbation.

5. Secondary instability and transition

We would like to determine to what extent the secondary instability mechanism discussed in the previous section is relevant to the transition process observed experimentally.

With respect to transition, the single most important parameter is the transitional Reynolds number. The critical Reynolds number predicted by secondary instability has already been shown to be in good agreement with the value of 500 that is observed in experiments. The next question is whether the secondary instability presented here saturates in an ordered state when it reaches finite amplitudes or whether it results in chaotic behaviour, and in general to what degree the resulting flow resembles turbulent flow structures that are observed in experiments. To answer these questions we have carried out a large numerical simulation at a Re^{δ} of 1000. The simulation was started from the results of the linear secondary instability calculations of the previous section at a time of $\Omega t = 4\pi/10$, at which point the three-dimensional perturbation had reached an energy of 0.015. At this time the resolution in the spanwise direction was increased and the simulation was continued with $P = 128$, $2N = 32$, $2M = 16$.

The results of this simulation are shown in figures 16 and 17. In figure 16, the normalized energy of the disturbances (relative to that of the mean flow) obtained by direct simulations is plotted as a function of the phase in the cycle. For comparison, in the same figure the normalized energy of the disturbances from the experimental run for turbulent oscillatory flow in a pipe at $Re^{\delta} = 1080$, $\Lambda = 10.6$ (from Akhavan *et al.* 1991) is also shown. It can be seen that there is excellent agreement between the simulations and experimental results for the second half-cycle during the simulation ($\pi < \Omega t < 2\pi$). In both cases the disturbances are seen to decay to small (but finite) levels of energy during the acceleration phase of the cycle, and to explosively grow prior to the start of the deceleration phase ($\Omega t \approx 3\pi/2$). As can be seen in figure 16, the results of the simulation for $0 < \Omega t < \pi$ are not identical to those for $\pi < \Omega t < 2\pi$. This is because the simulation was started from a low-resolution run at $\Omega t = 4\pi/10$. In particular the large peak in energy seen at $\Omega t = \pi/2$ is expected to be an artifact due to the low resolution of the initial conditions. These effects are eliminated as time progresses within the simulation, and the results for $\pi < \Omega t < 2\pi$ are expected to be representative of the behaviour of the flow in the periodic steady state.

Ensemble-averaged velocity profiles obtained from the simulation are compared to experimental profiles in figure 17. There is excellent agreement in the general shapes of the two profiles both during the acceleration and during the deceleration phases of the cycle. As discussed in Part 1 (Akhavan *et al.* 1991), the profiles for the acceleration phases are well described by laminar theory, while those during the deceleration phase can be described by a three-layer description consisting of a viscous sublayer, a logarithmic layer (with von Kármán constant = 0.4), and an outer wake near the centre of the channel if velocities are normalized with wall-friction velocities.

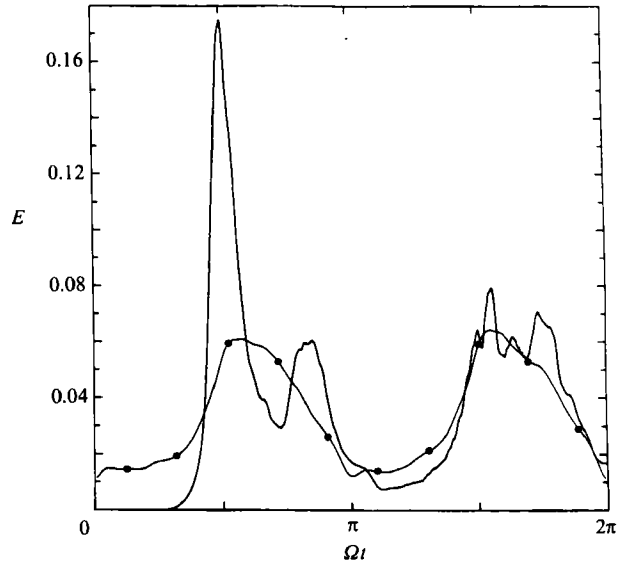

FIGURE 16. Phase variation of the overall energy of disturbances (normalized to that of the mean flow) from experiments (—●—) compared to results from the numerical simulation. ($Re^{\delta} = 1000$, $A = 10$.)

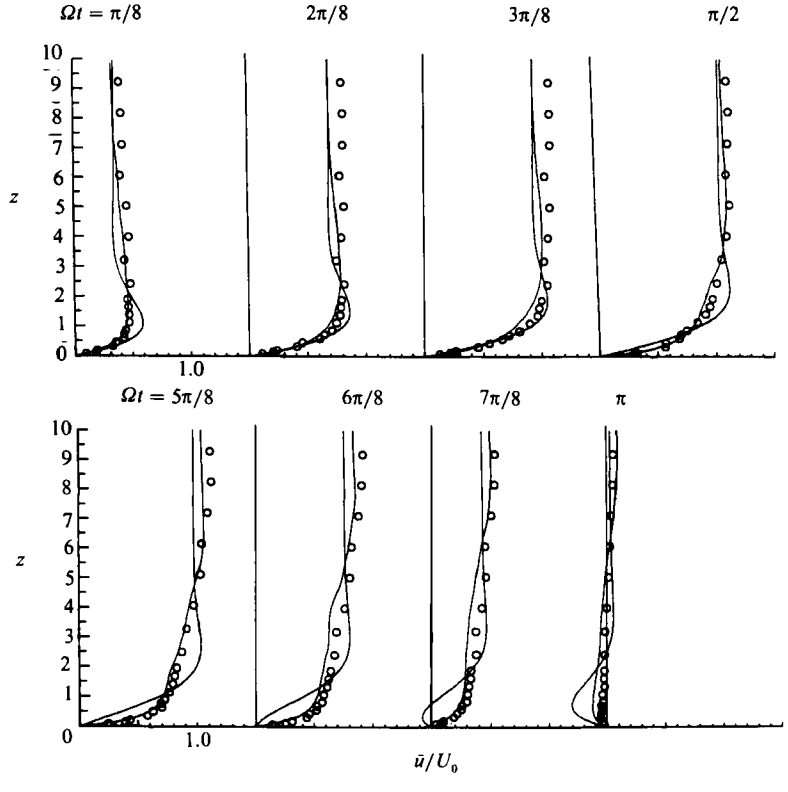

FIGURE 17. Ensemble-averaged velocity profiles from numerical simulations (solid lines) compared to experimental measurements (symbols) and to laminar theory. ($Re^{\delta} = 1000$, $A = 10$.)

6. Conclusions

The results presented in this work suggest that transition to turbulence in oscillatory Stokes layers can be explained by a secondary instability mechanism of two-dimensional finite-amplitude waves to three-dimensional infinitesimal disturbances. The value of the transitional Reynolds number, as well as the statistics of the resulting turbulent flow are well predicted by such a secondary instability mechanism.

We wish to thank Tony Patera for providing us with a version of his spectral code and for helpful discussions during the course of this work. This work was supported by NSF grant MEA-8313017. The numerical computations were performed on the CRAY-XMP of the Pittsburgh Supercomputer Center.

REFERENCES

AKHAVAN, R. 1987 An investigation of transition and turbulence in oscillatory Stokes layers. Ph.D. thesis, MIT, Cambridge, MA.

AKHAVAN, R., KAMM, R. D. & SHAPIRO, A. H. 1991 An investigation of transition to turbulence in bounded oscillatory Stokes flows. Part 1. Experiments. *J. Fluid Mech.* **225**, 395–422.

BAYLY, B. J. 1986 Three-dimensional instability of elliptical flow. *Phys. Rev. Lett.* **57**, 2160–2163.

COLLINS, J. I. 1963 Inception of turbulence at the bed under periodic gravity waves. *J. Geophys. Res.* **18**, 6007–6014.

COWLEY, S. J. 1987 High frequency Rayleigh instability of Stokes layers. In *Stability of Time Dependent and Spatially Varying Flows* (ed. D. L. Dwoyer & M. Y. Hussaini), pp. 261–275. Springer.

HALL, P. 1978 The linear stability of flat Stokes layers. *Proc. R. Soc. Lond.* A **359**, 151–166.

HERBERT, T. 1976 Periodic secondary motions in a plane channel. In *Proc. 5th Intl Conf. on Numerical Methods in Fluid Dynamics* (ed. A. I. Van de Vooren & P. J. Zandbergen). Lecture Notes in Physics, vol. 59, p. 235. Springer.

HERBERT, T. 1983 Secondary instability of plane channel flow to subharmonic three-dimensional disturbances. *Phys. Fluids* **26**, 871–874.

HERBERT, T. 1984 Analysis of the subharmonic route to transition in boundary layers. *AIAA Paper* 84-0009.

HINO, M., KASHIWAYANAGI, M., NAKAYAMA, A. & HARA, T. 1983 Experiments on the turbulence statistics and the structure of a reciprocating oscillatory flow. *J. Fluid Mech.* **131**, 363–400.

HINO, M., SAWAMOTO, M. & TAKASU, S. 1976 Experiments on transition to turbulence in an oscillating pipe flow. *J. Fluid Mech.* **75**, 193–207.

KERCZEK, C. VON & DAVIS, S. H. 1974 Linear stability theory of oscillatory Stokes layers. *J. Fluid Mech.* **62**, 753–773.

LANDMAN, M. J. & SAFFMAN, P. G. 1987 The three-dimensional instability of strained vortices in a viscous fluid. *Phys. Fluids* **30**, 2339–2342.

MERKLI, P. & THOMANN, H. 1975 Transition to turbulence in oscillating pipe flow. *J. Fluid Mech.* **68**, 567–575.

MONKEWITZ, P. A. & BUNSTER, A. 1987 The stability of the Stokes layer: visual observations and some theoretical considerations. In *Stability of Time Dependent and Spatially Varying Flows* (ed. D. L. Dwoyer & M. Y. Hussaini), pp. 244–260. Springer.

OBREMSKI, H. J. & MORKOVIN, M. V. 1969 Applications of a quasi-steady stability model to periodic boundary layer flow. *AIAA J.* **7**, 1298–1301.

OHMI, M., IGUCHI, M., KAKEHACHI, K. & MASUDA, T. 1982 Transition to turbulence and velocity distribution in an oscillating pipe flow. *Bull. JSME* **25**, 365–371.

ORSZAG, S. A. 1971 Accurate solution of the Orr–Sommerfeld stability equation. *J. Fluid Mech.* **50**, 689–703.

ORSZAG, S. A. & KELLS, L. C. 1980 Transition to turbulence in plane Poiseulle and plane Couette flow. *J. Fluid Mech.* **96**, 159–205.

ORSZAG, S. A. & PATERA, A. T. 1983 Secondary instability of wall-bounded shear flows. *J. Fluid Mech.* **128**, 347–385.

PIERREHUMBERT, R. T. 1986 Universal short-wave instability of two-dimensional eddies in an inviscid fluid. *Phys. Rev. Lett.* **57**, 2157–2159.

PIERREHUMBERT, R. T. & WIDNALL, S. E. 1982 The two- and three-dimensional instabilities of a spatially periodic shear layer. *J. Fluid Mech.* **114**, 59–82.

SERGEEV, S. I. 1966 Fluid oscillations in pipes at moderate Reynolds number. *Fluid Dyn.* **1**, 121–122.